# Terahertz spectroscopy of low-energy excitations in $Eu_{0.42}Sr_{0.58}MnO_3$

L. S. Kadyrov,[1,*] E. S. Zhukova,[1] V. I. Torgashev,[2] T. Zhang,[3] Z. V. Gagkaeva,[1] M. Dressel,[1,4] and B. P. Gorshunov[1]

[1]*Moscow Institute of Physics and Technology, Dolgoprudny, Moscow Region 141700, Russia*

[2]*Faculty of Physics, Southern Federal University, 5 Zorge, Rostov on Don 344006, Russia*

[3]*Key Laboratory of Materials Physics, Institute of Solid State Physics, Chinese Academy of Sciences, Hefei 230031, People's Republic of China*

[4]*1. Physikalisches Institut, Universität Stuttgart, D-70569 Stuttgart, Germany*

(Received 24 October 2017; revised manuscript received 22 November 2017; published 13 December 2017)

The origin of low-energy excitations in the polycrystalline $Eu_{0.42}Sr_{0.58}MnO_3$ manganite is explored by terahertz and infrared spectroscopies. The transition from the charge and/or orbital to antiferromagnetic order ($T_N$ = 130−140 K) is seen as smooth (spread over a temperature range from 50 to 100 K) decrease of free-carrier conductivity with the activation energy change from 86 meV (high temperatures) to 0.52 meV (low temperatures). A broad relaxation is observed at around 10 $cm^{-1}$ which we associate with the dynamics of free charge carriers in the presence of random localizing potential. We discover an absorption resonance at ≈50 $cm^{-1}$ below $T_N$ that is assigned to the formation of hybridized "acoustic phonon-magnon" quasiparticles.

DOI: 10.1103/PhysRevB.96.245120

## I. INTRODUCTION

In the large family of mixed valent manganese oxides $RE_{1-x}AE_xMnO_3$ (RE, rare-earth; AE, alkaline-earth elements), competition between various electronic phases with ordered spin, charge, and orbital subsystems results in a fascinating diversity of ground states and related phase transitions [1,2]. The ease with which one can switch between differently ordered phases by varying external parameters (temperature, magnetic field, stress, pressure, and doping) opens up broad prospects for practical use of the compounds and continues to further stimulate the ongoing active studies of the extremely rich palette of their physical properties. Comparability in strength of relevant order parameters is expected to reveal itself in existence of low-lying excited states. Detailed studies of such states can produce new information on fundamental properties of these complex systems. An effective means to perform such studies is provided by terahertz (THz) spectroscopy that allows one to probe the low-energy (fractions of meV up to several meV) excitations by monitoring the emergence and evolution of corresponding absorption features in the terahertz spectra—at frequencies from approximately 10 to 100 $cm^{-1}$. Applying a combination of a cw [3] and pulsed terahertz spectroscopic techniques enabled us to identify several types of absorption bands at 10−70 $cm^{-1}$ in overdoped $La_{1-x}Ca_xMnO_3[x(Ca) > 0.5]$ systems [4,5]. In the charge-ordered phase, absorption lines detected for commensurate $x$ values right below the charge-ordering temperature were assigned to acoustic phonons that become optically active by folding of the Brillouin zone (BZ). At lower temperatures, a strongly asymmetric extra absorption band was registered at frequencies corresponding to the position of the lowest-energy van Hove singularity in the reduced BZ. This band was assigned to the boson peak, i.e., to the excess of lattice vibrational states over the standard Debye contribution. It was shown that the folded phonons and the boson peak do not show up for incommensurate calcium contents when no distinct BZ folding exists. Later, several low-energy dispersion mechanisms were detected [6] in the ac conductivity and dielectric permittivity spectra of the colossal magnetoresistant manganite $Pr_{1-x}Ca_xMnO_3$ ($0.3 < x < 0.5$), belonging to the family that has a relatively narrow one-electron band. Here, the free-carrier conductivity was associated with small polarons coherently moving within a band several meV wide. An absorption band at 40−60 $cm^{-1}$ was associated with the transition between Stark-split $Pr^{3+}$ electron states, which gain optical activity due to coupling to acoustical phonons. In both families ($La_{1-x}Ca_xMnO_3$ and $Pr_{1-x}Ca_xMnO_3$), broad relaxation was observed in the THz-subterahertz (subTHz) spectra and its origin was assigned to delocalized carriers the response of which is governed by their dynamics in the presence of random localizing potential. The obtained results clearly indicate that soft excitations exist in manganites, the nature of which is connected with an interplay between spin, charge, orbital, and phonon subsystems. In this paper, we present the results of our investigations of terahertz-infrared (THz-IR) spectral response of another member of the perovskite manganites group, $Eu_{1-x}Sr_xMnO_3$. The compound is characterized by the mostly nonmagnetic ground state [7] except a narrow ferromagnetic metallic phase for $x$ = 0.38−0.47 with the lowest (first-order) transition temperature of about 40 K that is a consequence of the narrowed one-electron $e_g$ band. According to the phase diagram [8], for further increase of $x$ up to 0.7, spin-glass insulating, layered-type antiferromagnetic, and chained-type antiferromagnetic phases replace each other. For $0.55 < x < 0.59$, the charge and/or orbital ordering is settled above the antiferromagnetic phase [8,9]. A characteristic feature of these compounds is that they reveal dielectriclike temperature behavior of the electrical resistivity over the whole range accessible in experiment, and that they do not show any metal-to-insulator transition [8,9], except the mentioned range $0.38 < x < 0.47$ with an antiferromagnetic metallic phase. For compounds with $x$ close to 0.5, an application of external magnetic field suppresses the short-range charge or orbital ordering, leading to a significant increase of the nonmetal-metal transition temperature, from ≈40 K in zero field to >100 K at 7 T [8,10,11].

*kadyrov@phystech.edu

 

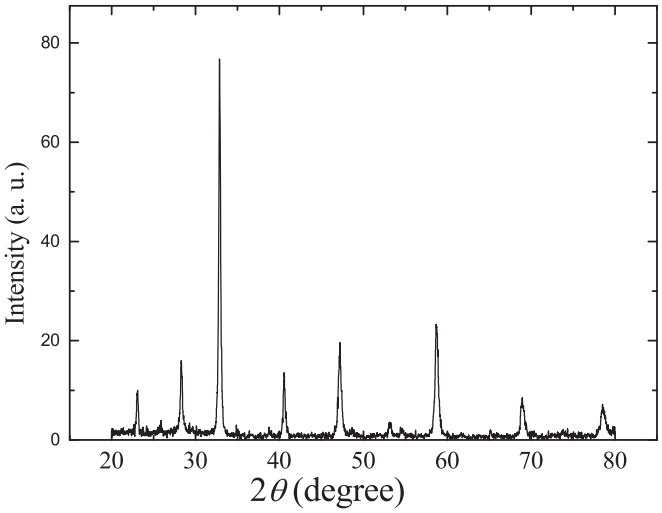


FIG. 1. The x-ray-diffraction patterns of $Eu_{0.42}Sr_{0.58}MnO_3$ at room temperature.

## II. EXPERIMENTAL DETAILS

As the subject of our investigations we have chosen the composition $Eu_{0.42}Sr_{0.58}MnO_3$ which is close to the boundary between chained antiferromagnetic and charge and/or orbital ordered phases [8]. Polycrystalline samples were prepared using a standard solid-state reaction method [12,13].The initial reagents $Eu_2O_3$, $SrCO_3$, and $MnO_2$ were preliminarily annealed: $Eu_2O_3$ at 1200 °C for 2 h, $SrCO_3$ and $CaCO_3$ at 500 °C for 3 h, and $MnO_2$ at 750 °C for 24 h. The latter process involved the transition from $MnO_2$ to $Mn_2O_3$. A mixture of the oxides was taken in the necessary stoichiometric proportion, thoroughly grinded in ethanol and annealed in four steps with intermediate grinding in ethanol every 20 h. The first stage was annealing at 850 °C for 20 h; the second stage was at 950 °C for 20 h; the third stage was at 1100 °C for 10 h. The product was pressed into pellets and sintered at 1300 °C for 20 h. Finally, the obtained samples were quenched by cooling to room temperature at a rate of 2.5 °C/min. To characterize the compounds, powder x-ray-diffraction measurements were made at room temperature on the MXP18AHF powder x-ray diffractometer (MAC Science Co., Ltd., Japan) using Cu *K*a radiation $\lambda = 1.54056$ Å. The observed diffraction patterns demonstrate that all samples are characterized with the *Pnma* space group indicating crystallization in the orthorhombic *Pnma* space group without any secondary or impurity phases (see Fig. 1).

For the THz-IR spectroscopic measurements, plane-parallel pellets of thickness 0.2–0.3 mm were prepared with both faces polished. At the THz frequencies, $\nu = 5-50\,\mathrm{cm}^{-1}$, the spectra of real and imaginary parts of complex dielectric permittivity $\varepsilon^*(\nu) = \varepsilon_1(\nu) + i\varepsilon_2(\nu)$ and real ac conductivity $\sigma(\nu)$ of $Eu_{0.42}Sr_{0.58}MnO_3$ polycrystals were *directly* determined by using the cw backward-wave oscillator (BWO) based [3] and pulsed time-domain THz spectrometers (where the BWO is the source of coherent and finely tunable THz radiation). Both spectrometers operate in the transmission mode and allow for calculations of all optical parameters of the material from the measured amplitude and phase of the complex transmission coefficient of a plane-parallel sample. In the IR range, up to $700\,\mathrm{cm}^{-1}$, standard Fourier-transform spectrometer Bruker 113V was employed for the measurements of reflection coefficient $R(\nu)$ of same samples. The broadband THz-IR spectra of $\sigma(\nu)$ and $\varepsilon_{1,2}(\nu)$ were obtained by performing the model dispersion analysis (see below) of the IR reflectivity spectra taking into account the directly determined THz spectra of $\sigma(\nu)$, $\varepsilon_1(\nu)$, and $\varepsilon_2(\nu)$ and the THz reflectivity *calculated* using the THz spectra $\varepsilon_1(\nu)$ and $\varepsilon_2(\nu)$. The results of the model analysis coincided with those obtained using the Kramers-Kronig analysis of the THz-IR reflectivity spectra. All measurements were performed at temperatures between 10 and 300 K using homemade optical cryostats with Mylar and polyethylene windows in the THz and IR ranges, respectively. Since the resistivity of the $Eu_{0.42}Sr_{0.58}MnO_3$ decreases while heating, we were not able to perform the THz transmissivity-based measurements above 200 K due to extremely low transmissivity of the pellet samples. At room temperature, only the spectrum of the THz bulk reflection coefficient was measured at frequencies $6-18\,\mathrm{cm}^{-1}$ as shown by dots in Fig. 2(a) where it merges well with the higher-frequency IR reflectivity; the Kramers-Kronig analysis of the merged THz and IR reflectivity provided us with broadband permittivity and conductivity spectra.

## III. EXPERIMENTAL RESULTS AND ANALYSIS

Spectra of the reflection coefficient, real permittivity, and ac conductivity are shown in Figs. 2(a)–2(c), respectively. Typical phononlike features are seen above $100\,\mathrm{cm}^{-1}$. During cooling, strong changes occur in the spectra below $100\,\mathrm{cm}^{-1}$. At $T = 300$ K, the spectra reveal behaviors that are typical for conducting materials in the limit of frequencies much smaller than the charge-carrier scattering rate [14,15]: the reflectivity increases towards low frequencies, and the permittivity and conductivity are almost frequency independent. While lowering the temperature, the reflection coefficient monotonically decreases in amplitude and flattens out at the value of $R \approx 0.44$ at $T = 10$ K. Note qualitatively different THz-IR dispersion of the reflectivity measured at 300 and 200 K. At 200 K the $R(\nu)$ spectrum has a *concave* shape and contains a pronounced flat part extending over a $40-100\text{-cm}^{-1}$ interval. Both spectral features are typical for dielectrics. At 300 K, the reflectivity spectrum has a *convex* shape and the flat part (present in the 200-K spectrum) is almost absent—a typical spectral shape of reflectivity of a conducting material. Metallic character of the room-temperature response of $Eu_{0.42}Sr_{0.58}MnO_3$ manifests itself also in the real permittivity spectrum $\varepsilon_1(\nu)$ that is shifted down relative to the 200-K spectrum since the corresponding contribution of free charge carriers is negative [14,15].

During cooling from 300 to 10 K, the lowest-frequency ($5\,\mathrm{cm}^{-1}$) conductivity decreases by more than two orders of magnitude with the dispersionless room-temperature behavior changed to almost monotonous increase at the lowest temperatures. The temperature evolution of the THz permittivity $\varepsilon_1(\nu)$ is pronouncedly nonmonotonous. When cooled from 300 to 200 K, the permittivity first increases almost twofold at $5\,\mathrm{cm}^{-1}$, always keeping a negative slope with frequency. At lower temperatures, the $\varepsilon_1(\nu)$ spectrum becomes nearly

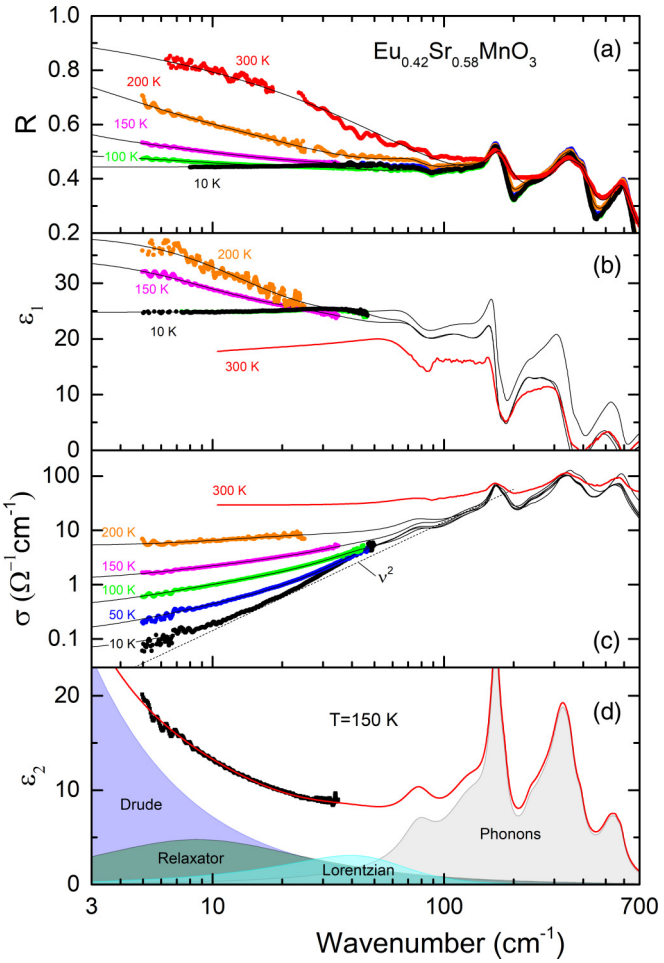


FIG. 2. Terahertz-infrared spectra of the reflection coefficient (a), real part of permittivity (b), and ac conductivity (c) of the $Eu_{0.42}Sr_{0.58}MnO_3$ polycrystalline sample measured at various temperatures as indicated. The solid lines display the results of the least-square fits of the measured spectra of the reflection coefficient together with the directly measured terahertz conductivity and permittivity spectra (dots below $\approx 50\,\mathrm{cm}^{-1}$) using Eqs. (1)–(3). The dashed line in panel (c) corresponds to the frequency squared dispersion of the lowest-frequency infrared phonon "tail." Panel (d) shows spectral contributions [Eqs. (1)–(3)] separately in the spectra of imaginary permittivity measured at $T = 150\,\mathrm{K}$.

dispersionless with the permittivity values of $\varepsilon_1(\nu) \approx 25$ at $T = 10\,\mathrm{K}$.

The detailed dispersion analysis of the obtained spectra allowed us to reveal the minimal set of dispersion mechanisms necessary for unambiguous description of the obtained data. These mechanisms are shown separately in Fig. 2(d) for the temperature $T = 150\,\mathrm{K}$. The phonon peaks were modeled by the standard Lorentzian expression

$$\sigma^*(\nu) = \sum_{k=1}^{12} \frac{0.5\Delta\varepsilon_k \nu_{0k}^2 \nu}{\nu\gamma_k + i\left(\nu_{0k}^2 - \nu^2\right)}, \tag{1}$$

where $\Delta\varepsilon$ is the dielectric contribution, $\nu_0$ is the resonance frequency, and $\gamma$ is the damping constant. The spectral dispersion connected with the response of free charge carriers was described by the Drude expression for the complex conductivity [14,15]:

$$\sigma^*_{\mathrm{Drude}}(\nu) = \frac{\sigma_0}{1 - \frac{i\nu}{\gamma_D}}, \tag{2}$$

where $\sigma_0$ is the dc conductivity and $\gamma_D$ is the charge-carrier scattering rate. Note that in the low-frequency limit, $\nu \ll \gamma_D$, Eq. (2) yields $\sigma(\nu) = \sigma_0 = \mathrm{const}$, $\varepsilon_2 = 2\sigma(\nu)/\nu \sim 1/\nu$, and $\varepsilon_1 = \mathrm{const}$. To account for the dispersion of permittivity $\varepsilon_1(\nu)$ and $\varepsilon_2(\nu)$ at THz frequencies most clearly seen at $T = 200\,\mathrm{K}$, a Debye relaxation approach [16] had to be used as is justified in the Discussion section. Complex dielectric permittivity is given by

$$\varepsilon^*_{\mathrm{rel}}(\nu) = \frac{\Delta\varepsilon_{\mathrm{rel}}}{1 + i\omega\tau_{\mathrm{rel}}}, \tag{3}$$

where $\Delta\varepsilon_{\mathrm{rel}}$ is the strength of the relaxation, $\tau_{\mathrm{rel}} = (2\pi\gamma_{\mathrm{rel}})^{-1}$ is the relaxation time, $\gamma_{\mathrm{rel}}$ is the relaxation frequency, and $\omega = 2\pi\nu$ is the circular frequency. Equations (1)–(3) were used to simultaneously describe the reflectivity, permittivity, and conductivity spectra within the least-square approach. During the analysis, to fully reproduce the spectra we had to introduce one extra absorption term represented by a Lorentzian that is located at $\approx 52\,\mathrm{cm}^{-1}$ [see Fig. 2(d)]. Presence of the corresponding absorption peak is most distinctly seen in the lowest-temperature (10 K) spectra, where directly measured THz permittivity $\varepsilon_1(\nu)$ shows clear local decrease in the range $35-50\,\mathrm{cm}^{-1}$ that is a clear fingerprint of an overdamped excitation, i.e., of an excitation with the damping exceeding resonance frequency [see Figs. 4(d) and 4(e)]. The excitation is also pronounced in the 10-K conductivity spectrum as a broad bump over the higher-frequency $\sim\nu^2$ phonon contribution [Fig. 2(c)]. Though at higher temperatures the mode is not so markedly visible in the measured spectra, to completely model these spectra we still had to keep the corresponding term up to 170 K with the parameters given in Figs. 4(d) and 4(e).

## IV. DISCUSSION

As noted above, the $Eu_{0.42}Sr_{0.58}MnO_3$ solid solution has an orthorhombic structure (space group *Pnma*) derived from the structure of a cubic perovskite. Such a structural type is described as a result of an antiferrodistorsive phase transition described by two order parameters associated with the rotational modes of the $MnO_6$ octahedra from the *M* and *R* points of the BZ of the cubic lattice [17–19]. The volume of the unit cell of the orthorhombic modification is four times that of the cubic one, leading to the activation of 45 new phonon modes from the *X*, *M*, and *R* points of the BZ of the cubic phase [20]. Schematically this process is shown in Fig. 3, where, as an example of dispersion phonon curves, the variant is taken of the cubic $SrMnO_3$ [21]. For an ideal cubic perovskite structure with five atoms in a unit cell, the phonon spectrum in the center of the BZ is constructed as follows [22]. $O_h{}^1(Pm3m)$ phase: $F_{2u}(\Gamma_8)$[silent] + $4F_{1u}(\Gamma_{10})$[IR]. During the $Pm3m \rightarrow Pnma$ phase transition (usually occurring at high temperatures), the symmetry analysis yields the following set of phonon modes. $D_{2h}{}^{16}(Pnma)$ phase: $7A_g$[Raman] + $5B_{1g}$[Raman] + $7B_{2g}$[Raman]+$5B_{3g}$[Raman]+$8A_u$[silent]+ $10B_{1u}$[IR] + $8B_{2u}$[IR] + $10B_{3u}$[IR].

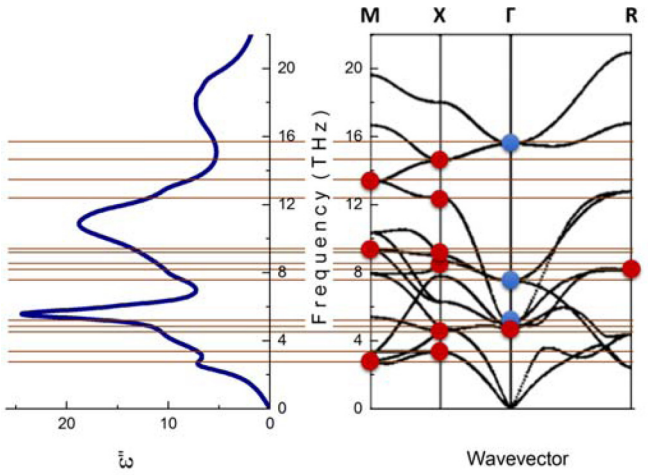


FIG. 3. A diagram showing the relationship between the observed phonons' density of states in the IR spectrum (left) of polycrystalline $Eu_{0.42}Sr_{0.58}MnO_3$ and the dispersion curves of the hypothetical cubic phase along the three directions in the Brillouin zone (right) [21]. The circles denote phonon modes that are activated in the infrared spectra of the lower-symmetry orthorhombic modification (space group *Pnma*).

At the Γ point of the cubic phase, the spectral density of optical phonons is formed by three triple-degenerate modes of the $F_{1u}$ type, that are active in IR absorption, and an IR-inactive $F_{2u}$ mode. In $Eu_{0.42}Sr_{0.58}MnO_3$ the low-frequency band (up to 200 $cm^{-1}$) in Fig. 2 reflects the antiphase motion of Eu and Sr relative to the $MnO_6$ octahedron. The band in the frequency range 200−400 $cm^{-1}$ is formed by modes involving Mn cations, and the higher-frequency band (400−600 $cm^{-1}$) is responsible for the movement of oxygen. (In general, the phonon modes involving displacements of the heavier atoms show up at lower frequencies than the mode involving lighter atoms.) This subdivision is due to the large difference in atomic masses of Eu and Sr cations and Mn relative to oxygen anions, but in reality each single fragment of the structure gives its partial contribution to each of the bands.

The distortion of the cubic perovskite cell requires three soft modes (at the *M*, *R*, and *X* points) for its description. The analysis reveals, however, that the observed displacements of atoms can be stated in terms of only two soft modes at the *M* and *R* points of the cubic BZ and that the modes at the *X* points should instead be considered to be second-order parameters [19]. The $Pm3m \rightarrow Pnma$ phase transition should enrich the Γ-point spectrum of the $Eu_{0.42}Sr_{0.58}MnO_3$ orthorhombic phase with the new lines as compared to the spectrum of an ideal perovskite. The degeneracy of the threefold degenerate modes at the center of the cubic phase is lifted, and the zone folding transfers the modes from the *M*, *R*, and *X* points at the boundary of the BZ to its center, as shown in Fig. 3. In this case we observe a structured appearance of each band. Table I presents the parameters of the observed phonon resonances obtained by spectral analysis described above. Only 12 individual phonon resonances were distinguished in the spectra with respect to the 25 expected ($9B_{1u} + 7B_{2u} + 9B_{3u}$); we can explain this finding by the polycrystalline nature of the studied samples, insignificant splitting of a part of the degenerate modes, and their relatively small dielectric contributions. Upon cooling down to 10 K, the phonon resonances get slightly sharper but their number remains unchanged. No new optical phonon modes are observed on cooling from 300 to 10 K through the antiferromagnetic transition at $T_N = 130-140$ K [9].

TABLE I. Parameters of phonon resonances observed in the THz-IR spectra of the $Eu_{0.42}Sr_{0.58}MnO_3$ polycrystalline sample at $T = 10$ K: $\nu_0$, frequency; $\gamma$, damping; $\Delta\varepsilon$, dielectric strength; $f = \Delta\varepsilon\nu_0^2$, oscillator strength. See Eq. (1).

| $\nu_0$ ($cm^{-1}$) | $\gamma$ ($cm^{-1}$) | $\Delta\varepsilon$ | $f = \Delta\varepsilon\nu_0^2$ |
|---|---|---|---|
| 77 | 30 | 1.6 | 9486 |
| 134 | 87 | 4.8 | 86189 |
| 168 | 23 | 2.4 | 67738 |
| 183 | 19.7 | 0.3 | 10047 |
| 238 | 46.8 | 0.7 | 39651 |
| 275 | 64 | 0.9 | 68063 |
| 328 | 85 | 3.5 | 376544 |
| 352 | 39 | 0.4 | 49562 |
| 389 | 49 | 0.5 | 75661 |
| 536 | 184 | 1.4 | 402214 |
| 551 | 133 | 0.6 | 182161 |
| 582 | 50 | 0.1 | 33872 |

At high temperatures (at 200 K and room temperature, Fig. 2) the free carrier response is seen in the spectra in the form of dispersionless ac conductivity. Below ≈200 K, the optical properties develop a pronounced non-Drude-like behavior, increasing conductivity $\sigma(\nu)$ and decreasing permittivity $\varepsilon_1(\nu)$. These behaviors could be indicative of a Mott-like hopping mechanism with $\sigma(\nu) \sim \nu^s (s < 1)$ and $\varepsilon_1 \sim \nu^{1-s}$ spectral fingerprints [16]. We feel, however, that this interpretation is not convincing for two reasons. First, our dc conductivity values $\sigma_0$ are in good agreement with the measured literature data [9]. Second, the observed temperature variation of the conductivity could not be described by expressions typical for hopping transport, $\sigma(T) \sim T^{1/(n+1)}$ (here *n* is the dimensionality of the conducting system [16]). From the obtained spectra we are not able to determine the values that characterize free carriers. In particular, due to intensive phonon bands, we could not identify the frequency where the free carrier conductivity is twice smaller than its dc value $\sigma_0$; according to Eq. (2), this frequency would provide us with the value of the carriers scattering rate $\gamma_D$. From our data only an estimate can be given: $\gamma_D > 200$ $cm^{-1}$. The inset in Fig. 4(a) demonstrates strong decrease of $\sigma_0$ when the sample is cooled down. The corresponding Arrhenius plot in Fig. 4(a) reveals the existence of two regimes with the high- and low-temperature activation energies of 86 and 0.52 meV, respectively. According to the phase diagram of $Eu_{1-x}Sr_xMnO_3$ [8], the temperature interval related to the crossover between these two regimes corresponds to the transition from the charge and/or orbital ordered phase to the antiferromagnetically ordered phase. As seen in Fig. 4, the transition is rather smooth and manifests in the conductivity change over a wide temperature interval, 50 to 100 K. The results clearly show that the transition leads to a pronounced change in the electrical transport mechanism. Since in manganites there exists a strong coupling of the spin subsystem to the charge, orbital, and phonon degrees of

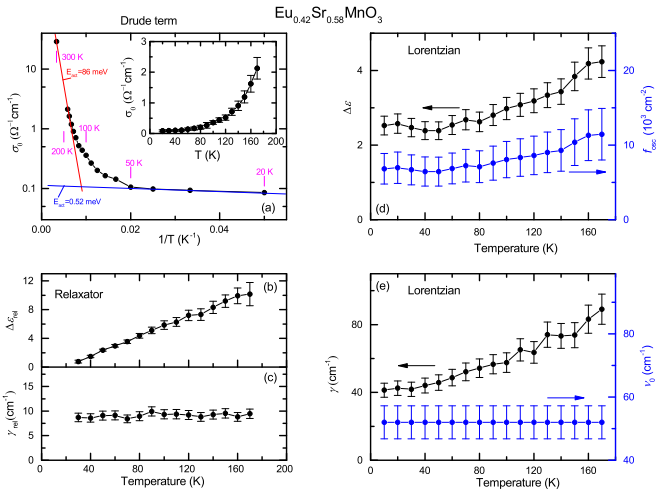


FIG. 4. Temperature dependence of the parameters of dispersion mechanisms observed in the THz-IR spectra of the $Eu_{0.42}Sr_{0.58}MnO_3$ polycrystalline sample and obtained by least-square fitting of the spectra presented in Fig. 2, as described in the text: dc conductivity $\sigma_0$ of free charge carriers (a), dielectric contribution $\Delta\varepsilon_{\rm rel}$ (b) and relaxation frequency $\gamma_{\rm rel}$ (c) of relaxation around 10 $\rm cm^{-1}$, dielectric contribution $\Delta\varepsilon$ and oscillator strength $f$ (d), and damping constant $\gamma$ and frequency $\nu_0$ of the Lorentzian at 52 $\rm cm^{-1}$ (e).

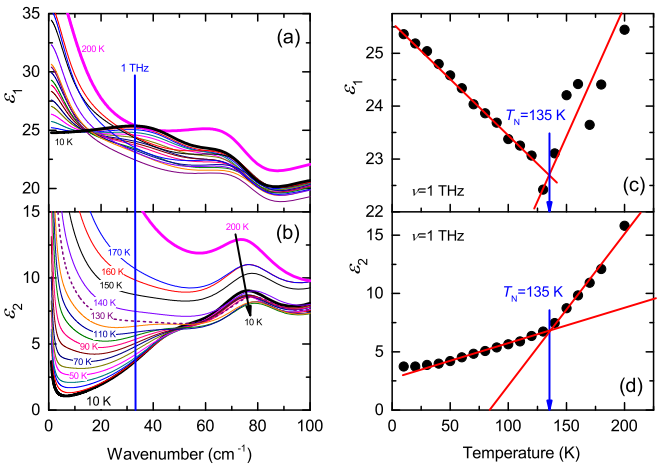


FIG. 5. (a, b) Terahertz spectra of real and imaginary parts of dielectric permittivity of polycrystalline $Eu_{0.42}Sr_{0.58}MnO_3$ measured at different temperatures. Only results of least-square fitting of experimental spectra are shown for clarity. Appearance below $T_N = 130-140$ K of a mode at 52 $\rm cm^{-1}$ is clearly seen. (c, d) Temperature dependences of real and imaginary parts of dielectric permittivity of polycrystalline $Eu_{0.42}Sr_{0.58}MnO_3$ at a frequency of 1 THz [spectra in panels (a) and (b)]. Kinks are clearly visible demonstrating appearance of the 52-$\rm cm^{-1}$ underdamped mode in the antiferromagnetically ordered phase.

freedom, an onset of an antiferromagnetic order can influence overlapping of electronic wave functions and thus transfer integrals (or carriers concentration $n$), and also scattering of charge carriers by phonons and magnetic centers. Recalling that the conductivity can be expressed as $\sigma_0 = ne^2(2\pi m^*\gamma_D)^{-1}$ ($m^*$ being carriers' effective mass and $e$ – their charge), we can conclude that the observed drastic change of the activation energy of the THz conductivity (by more than two orders of magnitude) during the transition can be caused by the variation of both concentration $n$ and scattering rate $\gamma_D$. As to the high-temperature phase ($T > 100$ K) where the charge and orbital orders are present, we can expect the temperature change of the scattering rate to be relatively small and the temperature dependence of the conductivity to be determined mainly by the variation of carrier concentration. Thus, the activation energy of 86 meV corresponds to certain minima where the charge carriers can reside. The nature of the minima is associated with lattice distortions produced by Mn-O-Mn bonds bending. We note that extrinsic effects might also play a certain role in the temperature variation of the conductivity; the disorder, for instance, is an important ingredient always present in manganites, in particular, in the $Eu_{1-x}Sr_xMnO_3$ family, as discussed below.

We believe that the presence of delocalized charge carriers is responsible for an additional excitation ["Relaxator" in Fig. 2(d)] that was discovered in the sub-THz spectra of $Eu_{0.42}Sr_{0.58}MnO_3$ and modeled by a relaxation term [Eq. (3)]. This is evidenced by a strong decrease of the dielectric strength $\Delta\varepsilon_{\rm rel}$ of the excitation upon cooling, as seen in Fig. 4(b); it accompanies the decrease of the free-carrier conductivity. We connect the origin of this relaxationlike excitation with the dynamical response of free charge carriers in the presence of a random potential relief with the minima where the carriers can reside. Depending on the temperature, certain fraction of the carriers will tend to occupy the deepest minima to minimize the total energy of the system. Such a process can be visualized in the spectra of dielectric permittivity and ac conductivity in the form of overdamped (relaxationlike) excitation. An example of this kind of dielectric response is given by ferroelectrics or dipolar glass relaxors [23] where the potential energy of the system is characterized by two or more minima [24,25]. The random potential in $Eu_{0.42}Sr_{0.58}MnO_3$ can be introduced by a quenched disorder present in the system due to different ionic radii of Sr and Eu ions [8,26]. Note that to describe the discussed relaxational process the Debye expression (3) is most adequate though it does not satisfy the sum rule and produces artificially high $\varepsilon"(\nu)$ and $\sigma(\nu)$ values for $\nu \gg \gamma$. Our analysis has shown that these excess values do not significantly influence the values of the parameters of all other terms that are analyzed in the present paper.

Finally, we want to discuss the origin of the 52-$\rm cm^{-1}$ resonance ["Lorentzian" in Fig. 2(d)]. It is seen in the spectra at temperatures below 130–140 K (see Fig. 5) in the form of a band that is overdamped [$\gamma > \nu_0$, Eq. (1)] at high temperatures but acquires a resonance shape ($\gamma < \nu_0$) after the transition to the antiferromagnetic phase with $T_N = 130-140$ K for $Eu_{0.42}Sr_{0.58}MnO_3$ [8]. Signatures of similar low-frequency excitation were observed in [27] where it was associated with the charge-density wave condensate. Since there are significant arguments against such interpretations (see [4,5,28–30]), we adhere to a different paradigm, which was previously presented in our papers on $La_{1-x}Ca_xMO_3$ manganites [4,5,30–32]. Charge ordering of $Mn^{3+}/Mn^{4+}$ at commensurate ion concentrations should lead to multiplication of the unit-cell volume of the compound, as was observed for $La_{1-x}Ca_xMO_3$ [33,34]. Then, the BZ of the resulting orthorhombic lattice

decreases in multiples of the value of the wave vector, which determines the ordering in the low-symmetry phase. In this case, there must be a "transfer" of modes from the inner and boundary points of the BZ to the center (wave vector $q = 0$) of the BZ of the new structural modification and, consequently, activation of new phonon absorption lines in the THz-IR spectra of the lower-symmetry modification. For $Eu_{1-x}Sr_xMnO_3$ single crystals, Tomioka *et al.* [8] find that in a wide range of compositions ($0.55 < x < 0.59$) the charge-orbital ordering with $q \sim 1/3$ is taking place and that the corresponding modulation is temperature dependent. Due to interconnection between magnetic, orbital, charge, and phonon subsystems, one expects an antiferrodistorsive phase transition with the $q = 1/3$ lattice superstructure and corresponding tripling of the unit cell and "ignition" of new $q = 0$ modes in the THz-IR spectra. Usually, in polycrystalline or ceramic samples it is not easy to visualize such folding modes at high frequencies since here—as a rule—the spectral response is "overloaded" by much more intense and broad bands corresponding to first-order optical phonon modes. On the other hand, in the 1–2-THz region where no such modes are present above the phase transition temperature, new bands corresponding to folded acoustic modes with $q \approx 0$ can be registered. It is important to note here that there is an anomalous feature in the low-frequency phonon dynamics of manganites, in particular, the presence of a flat dispersion region of the lower transverse branch of acoustic modes along the $\Sigma$ and $\Lambda$ directions in a wide range of wave vectors, $0.25 < q < 0.5$ [35]. Such behavior should give a high density of phonon states at the boundaries of the rhombic BZ, where in the case of $La_{1-x}Sr_xMnO_3$ the acoustic mode frequencies do not exceed 4 THz. Figure 5 clearly demonstrates that the mode at $52\,cm^{-1}$ (1.56 THz) appears in the antiferromagnetically ordered phase of $Eu_{0.42}Sr_{0.58}MnO_3$. The mode is too broad ($\gamma/\nu_0 = 0.8$ at 10 K) to be assigned to a pure magnon-type excitation. We thus believe that it is of a mixed origin associated with hybridized "acoustic phonon-magnon" interaction quasiparticles. It should be noted that signatures of this excitation are distinctly detected also above $T_N$, up to 180 K [Figs. 4(d) and 4(e)]. Here, however, it is heavily overdamped: its damping constant $\gamma$ is twice larger than the frequency $\nu_0$. We suggest that above $T_N$, in the charge and/or orbitally ordered phase, the excitation exists in a fluctuating regime reflecting existence of embryos of the lower-temperature antiferromagnetic phase that are generated owing to disorder, inhomogeneities, impurities, etc. Below $T_N$ the long-range magnetic order is settled and the excitation acquires a resonance character.

## V. CONCLUSIONS

In conclusion, terahertz-infrared spectroscopic studies of polycrystalline $Eu_{0.42}Sr_{0.58}MnO_3$ are performed at frequencies $5-700\,cm^{-1}$ and temperatures 10–300 K. It is shown that upon cooling down the free-carrier conductivity freezes out according to activation processes; their characteristic energies smoothly change from 86 to 0.52 meV between 50 and 100 K where the transition between the charge and/or orbitally and antiferromagnetically ordered phases occurs. Two low-energy excitations are discovered below $100\,cm^{-1}$. The Debye-like relaxation with the damping of $\approx 9\,cm^{-1}$ at $T = 30$ K is ascribed to free charge carriers the response of which is governed by their dynamics in presence of random localizing potential. The origin of excitation at $52\,cm^{-1}$ that is overdamped above $T_N$ and underdamped below $T_N$ is associated with the formation of hybridized acoustic phonon-magnon quasiparticles.

## ACKNOWLEDGMENTS

The paper was funded by RFBR under Research Project No. 16-32-00739 MOJI, Russian Ministry of Education and Science (Program 5 top 100), Southern Federal University (Grant No. VnGr-07/2017-23), and Moscow Institute of Physics and Technology visiting professor grant. We thank G. Untereiner for technical help and samples preparation.

[1] Y. Tokura, *Collosal Magnetoresistance Oxides* (Gordon and Breach, New York, 2000).
[2] J. M. D. Coey, M. V. Viret, and S. Von Molnar, Adv. Phys. **58**, 571 (2009).
[3] B. Gorshunov, A. Volkov, I. Spektor, A. Prokhorov, A. Mukhin, M. Dressel, S. Uchida, and A. Loidl, Int. J. Infrared Millimeter Waves **26**, 1217 (2005).
[4] T. Zhang, E. Zhukova, B. Gorshunov, D. Wu, A. S. Prokhorov, V. I. Torgashev, E. G. Maksimov, and M. Dressel, Phys. Rev. B **81**, 125132 (2010).
[5] B. Gorshunov, E. Zhukova, V. I. Torgashev, L. S. Kadyrov, E. A. Motovilova, F. Fischgrabe, V. Moshnyaga, T. Zhang, R. Kremer, U. Pracht, S. Zapf, and M. Dressel, Phys. Rev. B **87**, 245124 (2013).
[6] L. S. Kadyrov, T. Zhang, E. S. Zhukova, V. B. Anzin, V. G. Trotsenko, V. I. Torgashev, M. Dressel, and B. P. Gorshunov, Phys. Rev. B **93**, 184303 (2016).
[7] Y. M. Mukovskii, G. Hilscher, H. Michor, and A. M. Ionov, J. Appl. Phys. **83**, 7163 (1998).
[8] Y. Tomioka, R. Kumai, T. Ito, and Y. Tokura, Phys. Rev. B **80**, 174414 (2009).
[9] Y. Tomioka, X. Z. Yu, T. Ito, Y. Matsui, and Y. Tokura, Phys. Rev. B **80**, 094406 (2009).
[10] D. S. Rana, R. Nirmala, and S. K. Malik, Europhys. Lett. **70**, 376 (2005).
[11] P. Dutta, D. Das, S. Chatterjee, and S. Majumdar, J. Alloys Compd. **590**, 313 (2014).
[12] D. P. Kozlenko, L. S. Dubrovinsky, I. N. Goncharenko, B. N. Savenko, V. I. Voronin, E. A. Kiselev, and N. V. Proskurnina, Phys. Rev. B **75**, 104408 (2007).
[13] T. Qian, R. K. Zheng, T. Zhang, T. F. Zhou, W. B. Wu, and X. G. Li, Phys. Rev. B **72**, 024432 (2005).
[14] A. V. Sokolov, *Optical Properties of Metals* (Elsevier, New York, 1967).

[15] M. Dressel and G. Gruner, *Electrodynamics of Solids* (Cambridge University, Cambridge, England, 2002).
[16] A. K. Jonscher, *Dielectric Relaxation in Solids* (Chelsea Dielectric, London, 1983).
[17] W. Cochran and A. Zia, Phys. Status Solidi B **25**, 273 (1968).
[18] K. S. Aleksandrov and J. Bartolome, Phase Transitions **74**, 255 (2001).
[19] V. B. Shirokov and V. I. Torgashev, Crystallogr. Rep. **49**, 20 (2004).
[20] V. I. Torgashev, Y. I. Yuzyuk, V. B. Shirokov, V. V. Lemanov, and I. E. Spektor, Phys. Solid State **47**, 337 (2005).
[21] R. Sondena, S. Stolen, P. Ravindran, and T. Grande, Phys. Rev. B **75**, 214307 (2007).
[22] A. A. Volkov, G. A. Komandin, B. P. Gorshunov, V. V. Lemanov, and V. I. Torgashev, Phys. Solid State **46**, 927 (2004).
[23] R. Blinc, *Soft Modes in Ferroelectrics and Antiferroelectrics* (North-Holland, Amsterdam, 1974).
[24] N. F. Mott, *Metal-Insulator Transitions*, 2nd ed. (Taylor & Francis, London, 1990).
[25] N. F. Mott and E. A. Davis, *Electronic Process in Non-Crystalline Materials* (Oxford University, New York, 1971).
[26] L. M. Rodriguez-Martinez and J. P. Attfield, Phys. Rev. B **63**, 024424 (2000).
[27] P. Pandey, N. Awari, R. Rana, A. Singh, S. S. Prabhu, and D. S. Rana, Appl. Phys. Lett. **100**, 062408 (2012).
[28] R. Schmidt, Phys. Rev. B **77**, 205101 (2008).
[29] B. Fisher, J. Genossar, L. Patlagan, and G. M. Reisner, J. Magn. Magn. Mater. **322**, 1239 (2010).
[30] E. Zhukova, B. Gorshunov, T. Zhang, D. Wu, A. S. Prokhorov, V. I. Torgashev, E. G. Maksimov, and M. Dressel, Europhys. Lett. **90**, 17005 (2010).
[31] B. P. Gorshunov, E. S. Zhukova, E. G. Maksimov, A. S. Prokhorov, V. I. Torgashev, T. Zhang, D. Wu, and M. Dressel, JETP Lett. **91**, 336 (2010).
[32] V. G. Trotsenko, A. S. Mikheykin, V. B. Shirokov, A. G. Razumnaya, M. E. Marssi, B. P. Gorshunov, A. A. Bush, and V. I. Torgashev, Solid State Sci. **72**, 144 (2017).
[33] M. Pissas and G. Kallias, Phys. Rev. B **68**, 134414 (2003).
[34] M. Pissas, I. Margiolaki, K. Prassides, and E. Suard, Phys. Rev. B **72**, 064426 (2005).
[35] W. Reichardt and M. Braden, Physica B **263**, 416 (1999).